

## EFFECT OF THE SELENIUM CONTENT IN THE OPTICAL PROPERTIES OF THE KESTERITE $\text{Cu}_2\text{ZnSnS}_{4-x}\text{Se}_x$ PHASES

F. LÓPEZ-VERGARA<sup>a</sup>, A. GALDÁMEZ<sup>a</sup>, P. BARAHONA<sup>b</sup> and V. MANRÍQUEZ<sup>a</sup>

<sup>a</sup>Departamento de Química, Facultad de Ciencias, Universidad de Chile, Santiago, Chile

<sup>b</sup>Facultad de Ciencias Básicas, Universidad Católica del Maule, Talca, Chile

### ABSTRACT

Polycrystalline  $\text{Cu}_2\text{ZnSnS}_{4-x}\text{Se}_x$  ( $X=1, 2, 3$ ) compounds were synthesized by conventional solid-state reactions. The samples were characterized by powder X-ray diffraction (XRD), energy-dispersive X-ray analysis (SEM-EDS), Raman spectroscopy, diffuse reflectance UV-vis and Photoluminescence. All of phases crystallize in the tetragonal kesterite-type structure. The powder X-ray diffraction (XRD) patterns were indexed in the space group  $I\bar{4}$ . No secondary phases were detected in XRD patterns. The results from diffuse reflectance show band gap between 1.26 - 1.17 eV, when S is gradually replaced by Se. The PL spectrum of  $\text{Cu}_2\text{ZnSnS}_{4-x}\text{Se}_x$  phases shows nearly symmetrical band, which shifted linearly to the lower energy with increasing Se content. The selenized (CZTSSe) phases are promising candidates to be used as absorbing material in solar cells

### INTRODUCTION

In recent decades, the study of new photovoltaic (PV) materials for the development of more efficient and lower-cost solar cells has become the subject of an impressive field of research in physics, and solid state chemistry [1].

The quaternary semiconductor Copper-Zinc-Tin-Sulfur  $\text{Cu}_2\text{ZnSnS}_4$  (CZTS) is the focus of new materials with great potential for its application as absorbent materials for solar cells [2-6]. The CZTS phase has interesting physical properties suitable for photovoltaic applications, namely, optimum band gap of ~1.5 eV and its absorption coefficient of  $\sim 10^4 \text{ cm}^{-1}$  [7-11]. These values are similar to those of  $\text{Cu}(\text{In,Ga})(\text{S,Se})_2$  (CIGS), that is one of them more successful thin-film PV materials, of commercial use, with power conversion efficiencies (PCEs) of nearly 20% [12-14]. However, unlike the CIGS, the CZTS phase is formed by elements that are abundant, cheap and of low toxicity, in addition, the CZTS-PV devices shown PCEs of up to 6.7% [13-15].

In the last years, has been informed the preparation of CZTS nanoinks, for the preparation of high quality thin-films of CZTS and CZTSSe, suitable for use in solar cells [16]. The devices fabricate with thin-films nanoparticles of CZTS have shown the power conversion efficiency (PCE) of 8.4% [17-18]. Also, it has been reported that Wurtzite nanoparticle films of CZTS presents a phase transformation to kesterite phase, when sintered in selenium vapor at 500°C. The resulting thin-film of the selenized  $\text{Cu}_2\text{ZnSn}(\text{S,Se})_4$  (CZTSSe) presents a significant improvement in performance as dye solar cells [19]. The device built with selenized kesterite CZTSSe nanoparticle inks presents a PCE of 9.15% and this value has been improved to 9.4% by partial doping of Sn with Ge [20-22].

We have previously reported on the synthesis, structural characterization and magnetic properties of;  $\text{Cu}_2\text{Mn}_{1-x}\text{Co}_x\text{SnS}_4$  with kesterite structure,  $\text{Cu}_2\text{Mn}_x\text{Fe}_{1-x}\text{SnS}_4$  and  $\text{Cu}_2\text{Fe}_{1-x}\text{Co}_x\text{SnS}_4$  solid solutions [23-25]. The aim of this work is to study the effect on the physics properties of the Selenium content in the phase CZTS. In particular we report here the synthesis, characterizations and the optical properties of the  $\text{Cu}_2\text{ZnSnS}_3\text{Se}$ ,  $\text{Cu}_2\text{ZnSnS}_2\text{Se}_2$  and  $\text{Cu}_2\text{ZnSnSSe}_3$ .

### EXPERIMENTAL

#### Synthesis

The synthesis of Polycrystalline  $\text{Cu}_2\text{ZnSnS}_{4-x}\text{Se}_x$  (with  $x = 1, 2, 3$ ) compounds were performed on solid state by the ceramic method.  $\text{Cu}_2\text{ZnSnS}_3\text{Se}$ ,  $\text{Cu}_2\text{ZnSnS}_2\text{Se}_2$  and  $\text{Cu}_2\text{ZnSnSSe}_3$  were prepared by reaction of the high-purity element powders (99.99%, Aldrich) in stoichiometric amounts. All manipulations were carried out under an argon atmosphere. The reaction mixtures were sealed in evacuated quartz ampoules, placed in a programmable furnace, and heated at 850 °C for 72 h, and then cooled by quenching in liquid nitrogen. The reaction products appeared to be air- and moisture-stable over several weeks.

#### SEM-EDS analysis

The chemical compositions of the powder samples were determined by scanning electron microscopy (SEM) with the aid of energy-dispersive X-ray analysis (SEM-EDS) using a JEOL 400 system equipped with an Oxford Link ISIS microanalyzer. The working distance was 35 mm and the accelerating

voltage was 22.5kV. The samples were mounted on double-sided carbon tape, which adhered to an aluminum specimen holder. The EDS spectra were collected for 60s.

#### Powder X-ray diffraction measurements

Powder XRD patterns were collected at room temperature using a Bruker D8 advanced powder diffractometer, with  $\text{CuK}\alpha$  radiation ( $\lambda = 1.541 \text{ \AA}$ ) in the range of  $5^\circ < 2\theta < 80^\circ$  at  $0.01^\circ/\text{s}$ .

#### Raman spectroscopy

The Raman spectra of powder samples were recorded in the frequency range  $100\text{--}1800 \text{ cm}^{-1}$  using a micro-Raman Renishaw system 1000 equipped with a microscope Leica-DMLM. The spectra data were collected at room temperature with laser line of 633 nm and laser power of ~1 mW.

#### Diffuse reflectance UV-vis measurements

The diffuse reflectance UV-vis spectra were recorded using a Perkin Elmer UV-visible spectrophotometer.  $\text{BaSO}_4$  powder was used as reference at all energies (100% reflectance). Reflectance measurements were converted to absorption spectra using the Kubelka-Munk function.

#### Photoluminescence measurements (PL)

PL spectra were recorded by using a LabRam HR800-UV Horiba Jobin Yvon spectrometer with a laser excitation source solid state laser (line 532nm and 1064 nm) system with CCD detector (InGaAs diode). In all cases, spectra were measured in backscattering configuration; excitation and light collection was made through an Olympus metallographic microscope, with a laser spot on the sample of ~1  $\mu\text{m}$ .

### RESULTS AND DISCUSSION

The chemical compositions of the powder samples were determined using EDS analysis on polished surfaces of the pelletized samples. The backscattered image and EDS analysis (chemical maps of several areas) revealed that the samples were uniform throughout the scanned region (Fig 1). It was found that the average concentrations of Cu, Zn, Sn, S and Se elements were close to the nominal compositions (Table 1).

It is known that CZTS crystallizes in a tetragonal kesterite structure (space group  $I\bar{4}$ ), which consisting a *ccp* array of sulfur anions, with metal cations occupying one half of the tetrahedral interstitial sites within the S sublattice. The crystal structure of  $\text{Cu}_2\text{ZnSnS}_4$ ,  $\text{Cu}_2\text{ZnSnS}_3\text{Se}$ ,  $\text{Cu}_2\text{ZnSnS}_2\text{Se}_2$  and  $\text{Cu}_2\text{ZnSnSSe}_3$  can be represented by the cation-centered tetrahedral,  $\text{MQ}_4$  (with  $\text{M} = \text{Cu, Zn and Sn}$ ;  $\text{Q} = \text{S, Se}$ ), arranged in such a way that all polyhedra are oriented in the same direction and connected to each other at the corners, as illustrated in Figure 2. Moreover, S and Se atoms present a disorder in the occupation (same crystallographic site) at the corner of the  $\text{MQ}_4$  tetrahedral. The experimental XRD patterns of the polycrystalline  $\text{Cu}_2\text{ZnSnS}_{4-x}\text{Se}_x$  phases (Fig. 3) were fully indexed in I-4 space group. All phases are isostructural and adopted the kesterite-type structure. The final structural parameters are summarized in Table 2. As expected, the cell parameters obey Vegard's law (Fig. 4), in according with the gradual increase of the volume of the cell lattice as sulfur was replaced by selenium, in line with the increased of the anions radii. No secondary phases or impurity peaks were detected in XRD pattern of  $\text{Cu}_2\text{ZnSnS}_{4-x}\text{Se}_x$ .

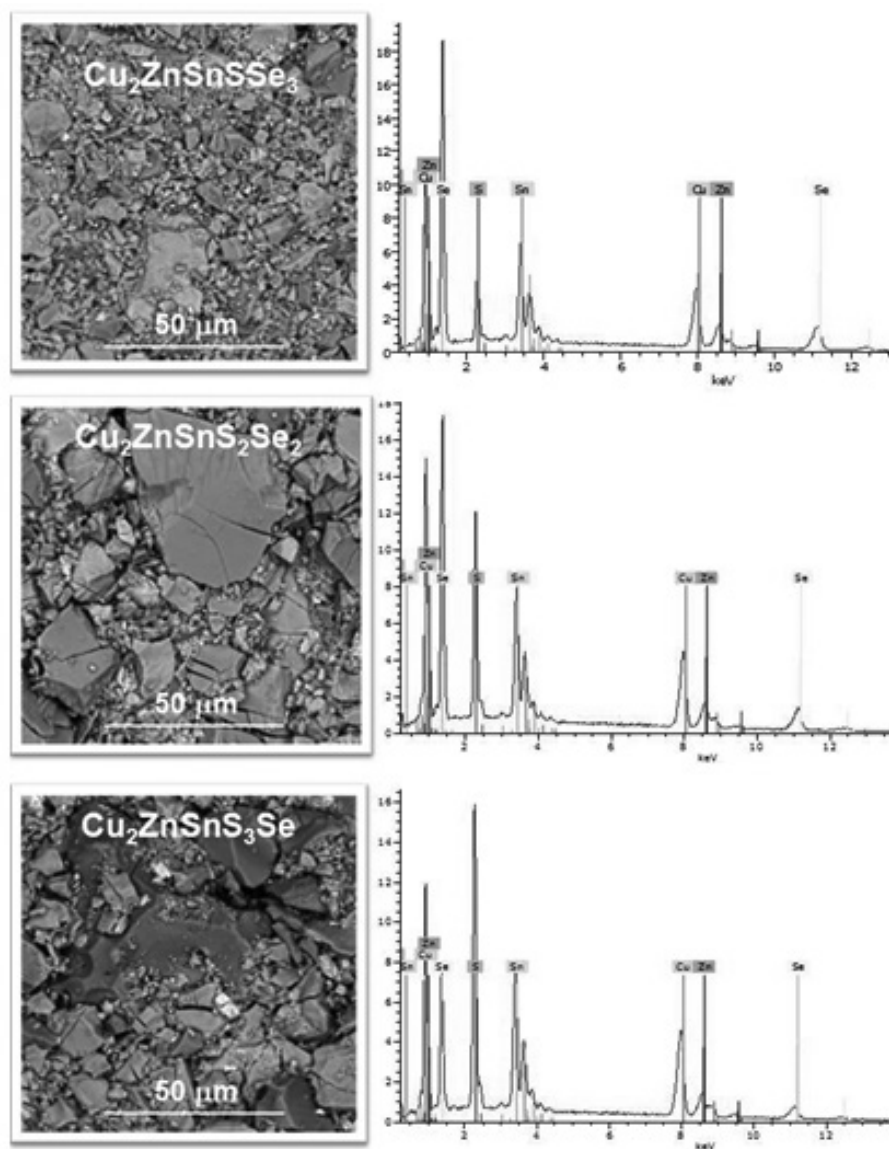


**Fig. 1** (SEM) micrograph: Backscattering electron image (left) and the corresponding EDS spectral analysis (right) of the solid solutions  $\text{Cu}_2\text{ZnSn}_{4-x}\text{Se}_x$

**Table 1.** Chemical composition analysis (% mass) of  $\text{Cu}_2\text{ZnSn}_{4-x}\text{Se}_x$  and end-members

Fase	Cu	Zn	Sn	S	Se	Experimental
$\text{Cu}_2\text{ZnSnS}_4$	28.9/34.5	14.9/18.2	27.0/21.7	29.2/25.5	---	$\text{Cu}_{2.4}\text{Zn}_{1.2}\text{Sn}_{0.8}\text{S}_{3.5}$
$\text{Cu}_2\text{ZnSnS}_3\text{Se}$	26.1/30.1	13.4/10.9	24.4/24.0	19.8/15.8	16.2/19.1	$\text{Cu}_{2.3}\text{Zn}_{0.8}\text{Sn}_{1.0}\text{S}_{2.4}\text{Se}_{1.2}$
$\text{Cu}_2\text{ZnSnS}_2\text{Se}_2$	23.8/24.9	12.3/10.9	22.3/22.4	12.0/11.2	29.6/30.4	$\text{Cu}_{2.1}\text{Zn}_{0.9}\text{Sn}_{1.0}\text{S}_{1.9}\text{Se}_{2.0}$
$\text{Cu}_2\text{ZnSnSSe}_3$	21.9/22.4	11.3/13.2	20.5/19.8	5.5/4.6	40.8/38.3	$\text{Cu}_{2.0}\text{Zn}_{1.2}\text{Sn}_{1.0}\text{S}_{0.8}\text{Se}_{2.8}$
$\text{Cu}_2\text{ZnSnSe}_4$	20.3/20.8	10.4/8.6	18.9/15.45	---	50.4/55.1	$\text{Cu}_{2.0}\text{Zn}_{0.8}\text{Sn}_{0.8}\text{Se}_{4.4}$

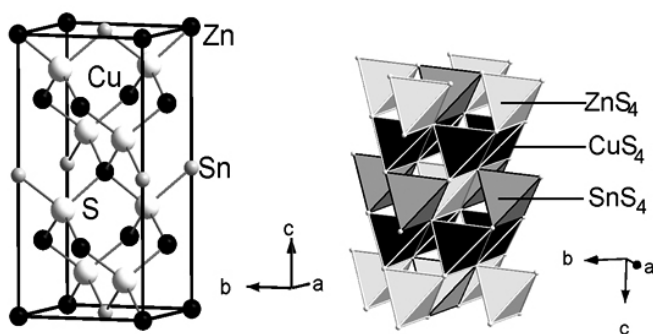


Fig.2. Unit cell of the  $\text{Cu}_2\text{ZnSnS}_4$  structure viewed along [010]

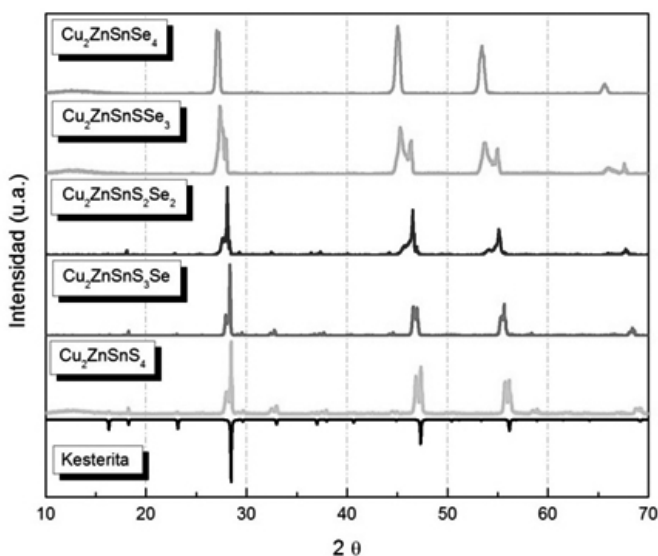


Fig.3. Experimental X-ray powder diffraction patterns of  $\text{Cu}_2\text{ZnSnS}_{4-x}\text{Se}_x$

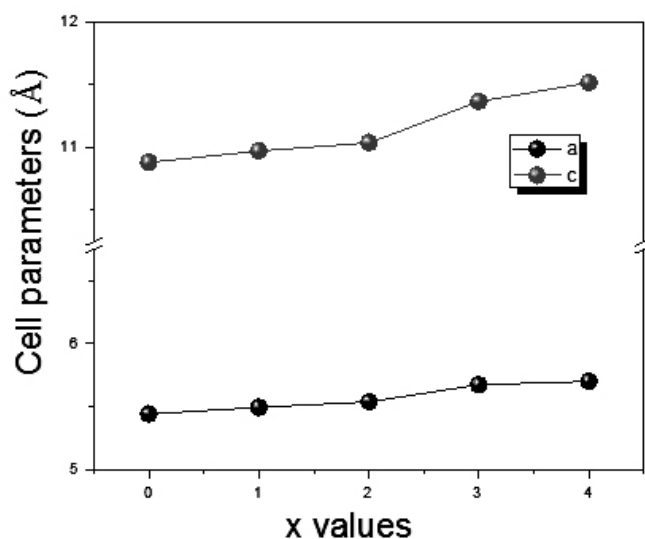


Fig.4. Vegard's law of  $\text{Cu}_2\text{ZnSnS}_{4-x}\text{Se}_x$  phases

Table 2 Cell parameters data for  $\text{Cu}_2\text{ZnSnS}_{4-x}\text{Se}_x$  and end-members.

Fase	a (Å)	c (Å)	Vol. (Å <sup>3</sup> )
$\text{Cu}_2\text{ZnSnS}_4$	$5.422 \pm 0.005$	$10.880 \pm 0.001$	319.861
$\text{Cu}_2\text{ZnSnS}_3\text{Se}$	$5.493 \pm 0.004$	$10.971 \pm 0.003$	331.064
$\text{Cu}_2\text{ZnSnS}_2\text{Se}_2$	$5.539 \pm 0.005$	$11.037 \pm 0.002$	338.681
$\text{Cu}_2\text{ZnSnSSe}_3$	$5.674 \pm 0.004$	$11.365 \pm 0.001$	365.936
$\text{Cu}_2\text{ZnSnSe}_4$	$5.701 \pm 0.010$	$11.513 \pm 0.008$	374.137

The Raman spectra of powder samples at room temperature are shown in figure 5. The spectra of CZTS is characterized by one strong line centered around  $335 \text{ cm}^{-1}$ , and a weak at  $285 \text{ cm}^{-1}$ , which can be assigned to the  $A1$  vibration mode, aside from a weak contribution at  $370 \text{ cm}^{-1}$  assigned to the  $B2$  mode [26, 27]. The vibrations of the  $A1$  mode can be viewed as a “breathing” mode of  $\text{MS}_4$  ( $M = \text{Cu, Zn and Sn}$ ) tetrahedra. This vibrational mode can be understood as the expansion or contraction of the  $M-S$  bonds, simultaneously triggered by sulfur atoms placed at the vertices of the tetrahedra. The Raman spectrum of CZTSe is characterized by two main peaks, which also can be assigned to the  $A1$  vibration mode, at  $175 \text{ cm}^{-1}$  and  $145 \text{ cm}^{-1}$ , while the sulfoselenide, which contains both S and Se at the anion sites in the crystal lattice, presents broadening peaks corresponding to  $A1$  modes from both end-members.

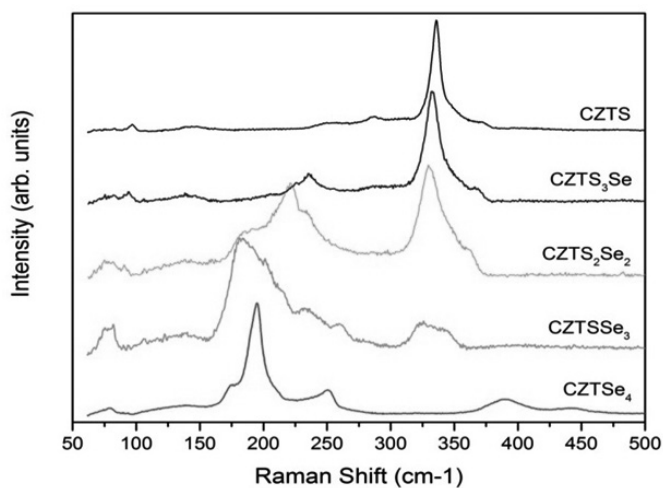


Fig.5. Room temperature Raman spectrum of polycrystalline  $\text{Cu}_2\text{ZnSn}(\text{S,Se})_4$  phases.

The optical properties of the  $\text{Cu}_2\text{ZnSn}(\text{S,Se})_4$  phases were measured by UV-vis. The results from spectra for  $\text{Cu}_2\text{ZnSnSSe}_3$ ,  $\text{Cu}_2\text{ZnSnS}_2\text{Se}_2$  and  $\text{Cu}_2\text{ZnSnS}_3\text{Se}$  phases show band gaps between  $1.17 - 1.26 \text{ eV}$ , when Se is gradually replaced by S, these values are consistent with the reported values of approximately  $1.0 \text{ eV}$  for CZTSe and  $1.44 \text{ eV}$  for CZTS [26, 28].

The PL spectrum of  $\text{Cu}_2\text{ZnSnS}_{4-x}\text{Se}_x$  shows nearly symmetrical band, it is possible to observe that there is a shift from  $1.39 \text{ eV}$  to  $1.26 \text{ eV}$  of the bands, consistent with the increasing of selenium, these values are according with the data obtained from of UV-Vis measurements, and also with the corresponding values reported in literature for the quaternary  $\text{Cu}_2\text{ZnSnS}_4$  and  $\text{Cu}_2\text{ZnSnSe}_4$  phases [4]. Tanaka et al. [29] attributed the detected broad PL band between  $1.1-1.45 \text{ eV}$  to donor-acceptor pair recombination

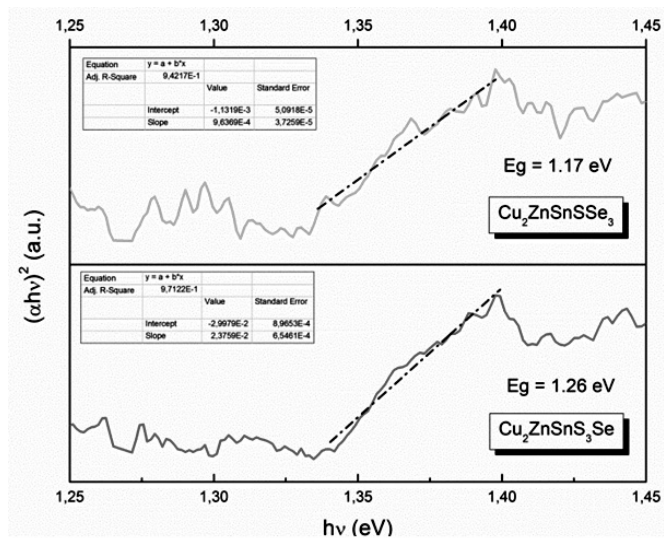


Fig.6. The optical absorption spectrum of  $\text{Cu}_2\text{ZnSnS}_{3-x}\text{Se}_x$  phases

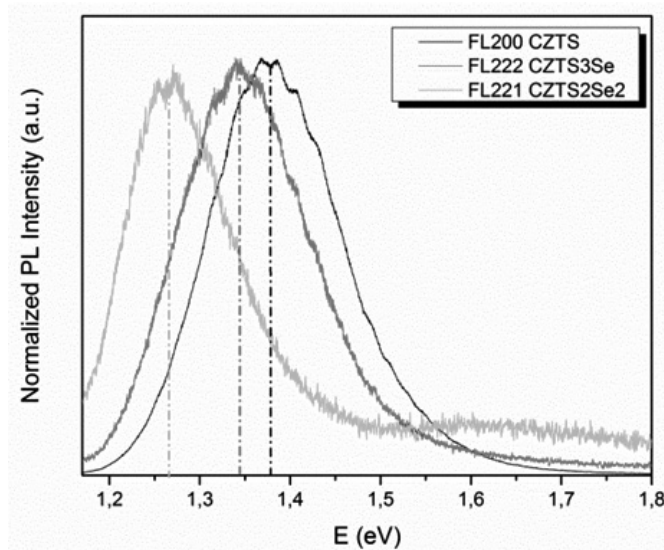


Fig.7. Photoluminescence PL spectra of polycrystalline  $\text{Cu}_2\text{ZnSn}(\text{S,Se})_x$  phases.

### CONCLUSIONS

The solid  $\text{Cu}_2\text{ZnSnS}_{3-x}\text{Se}_x$  ( $x = 1,2,3$ ) phases were obtained by conventional solid-state synthesis method. The SEM-EDS analysis confirms the chemical compositions. The Raman spectra were dominated by the peaks assigned to the A1 vibration mode, the broadening of these peaks can be attributed to the disorder effects related to  $\text{SnQ}_4$  and  $\text{MQ}_4$  ( $\text{M} = \text{Cu}^{2+}$  and  $\text{Zn}^{2+}$ ;  $\text{Q} = \text{S, Se}$ ) tetrahedra. The results of diffuse reflectance combined with photoluminescence show band-gap values  $E_g$  between 1.26 to 1.17 eV, the experimental observation have showed that the band gap of CZTS decreased linearly when S is gradually replaced by Se. Thus, the S/Se ratio can be used to adjust an optimal band gap in the CZTSSe phase.

### ACKNOWLEDGMENTS

The authors thank the financial support of FONDECYT Post-doctoral project 3140520, and the Vibrational Spectroscopy Laboratory of the Facultad de Ciencias, Universidad of Chile.

### REFERENCES

- [1] H. Katagiri, *Thin Solid Films*, **426**,480–481 (2005)
- [2] K. Ito and T. Nakazawa, *Jpn. J. Appl. Phys.* **27**, 2094 (1988)
- [3] K. Jimbo, R. Kimura, S. Yamada, W. S. Maw, H. Araki, K. Oishi, and H. Katagiri, *Thin Solid Films*, **515**, 5997 (2007).
- [4] M. Altosaar, J. Raudoja, K. Timmo, M. Danilson, M. Grossberg, J. Krustok, and E. Mellikov, *Phys. Stat. Sol. (a)* **205**, No. 1, 167–170 (2008)
- [5] S. Delbos, *EPJ Photovoltaics* **3**, 35004 (2012)
- [6] A. Walsh, S. Chen, S-H. Wei and X-G. Gong, *Adv. Energy Mater.*, **2**, 400–409 (2012)
- [7] Todorov, T.; Kita, M.; Carda, J.; Escribano, P., *Thin Solid Films*, **517**, 2541–2544 (2009)
- [8] Yeh, M. Y.; Lee, C. C.; Wu, D. S., *J. Sol-Gel Sci. Technol.*, **52**, 65–68 (2009)
- [9] Seol, J. S.; Lee, S. Y.; Lee, J. C.; Nam, H. D.; Kim, K. H., *Sol. Energy Mater. Sol. Cells*, **75**, 155–162 (2003)
- [10] Kishore Kumar, Y. B.; Suresh Babu, G.; Uday Bhaskar, P.; Sundara Raja, V., *Sol. Energy Mater. Sol. Cells*, **93**, 1230–1237 (2009)
- [11] X. Song, X. Ji, M. Li, W. Lin, X. Luo, H. Zhang, *Int. J. Photoenergy*, 1–11 (2014)
- [12] Chet Steinhagen, Matthew G. Panthani, Vahid Akhavan, Brian Goodfellow, Bonil Koo, and Brian A. Korgel, *J. AM. CHEM. SOC.*, **131**, 12554–12555 (2009)
- [13] Katagiri, H.; Jimbo, K.; Maw, W. S.; Oishi, K.; Yamazaki, M.; Araki, H.; Takeuchi, A., *Thin Solid Films*, **517**, 2455 (2009)
- [14] Repins, I.; Contreras, M. A.; Egaas, B.; DeHart, C.; Scharf, J.; Perkins, C. L.; To, B.; Noufi, R., *Prog. PhotoVoltaics*, **16**, 235 (2008)
- [15] Wadia, C.; Alivisatos, A. P.; Kammen, D. M., *Environ. Sci. Technol.*, **43**, 2072 (2009)
- [16] J. Zhong, Z. Xia, C. Zhang, B. Li, X. Liu, Y-B. Cheng, and J. Tang, *Chem. Mater.*, **26**, 3573–3578 (2014)
- [17] Repins, I.; Beall, C.; Vora, N.; DeHart, C.; Kuciauskas, D.; Dippe, P.; To, B.; Mann, J.; Hsu, W.-C.; Goodrich, A.; Noufi, R., *Sol. Energy Mater. Sol. Cells*, **101**, 154–159 (2012)
- [18] Shin, B.; Gunawan, O.; Zhu, Y.; Bojarczuk, N. A.; Chey, S. J.; Guha, S., *Prog. Photovoltaics: Res. Appl.*, **21**, 72–76 (2013)
- [19] W.-C. Yang, C. K. Miskin, C. J. Hages, E. C. Hanley, C. Handwerker, E. A. Stach and R. Agrawal, *Chem. Mater.*, **26**, 3530–3534 (2014)
- [20] Miskin, C. K.; Yang, W.-C.; Hages, C. J.; Carter, N. J.; Joglekar, C. S.; Stach, E. A.; Agrawal, R., *Prog. Photovoltaics: Res. Appl.*, **24**, 2472 (2014)
- [21] Guo, Q.; Ford, G. M.; Yang, W.-C.; Hages, C. J.; Hillhouse, H. W.; Agrawal, R., *Sol. Energy Mater. Sol. Cells*, **105**, 132–136 (2012)
- [22] Hages, C. J.; Levenco, S.; Miskin, C. K.; Alsmeier, J. H.; Abou-Ras, D.; Wilks, R. G.; Bär, M.; Unold, T.; Agrawal, R., *Prog. Photovoltaics: Res. Appl.*, **24**, 2442 (2013)
- [23] F. López-Vergara, A. Galdámez, V. Manríquez, P. Barahona, O. Peña, *J. Solid State Chem.* **198**, 386-391 (2013)
- [24] F. López-Vergara, A. Galdámez, V. Manríquez, P. Barahona, O. Peña, *Phys. Status Solidi* **251**, 958-964 (2014)
- [25] F. López-Vergara, A. Galdámez, V. Manríquez, Guillermo González, *Solid State Sciences*, **49**, 54-60 (2015)
- [26] Chen, S.; Walsh, A.; Yang, J.-H.; Gong, X. G.; Sun, L.; Yang, P.-X.; Chu, J.-H.; Wei, S.-H., *Phys. Rev. B*, **83**, 125201 (2011)
- [27] Fontane, X.; Calvo-Barrio, L.; Izquierdo-Roca, V.; Saucedo, E.; Perez-Rodriguez, A.; Morante, J. R.; Berg, D. M.; Dale, P. J.; Siebentritt, S., *Appl. Phys. Lett.*, **98**, 181905 (2011)
- [28] H. Matsushita, T. Maeda, A. Katsui, and T. Takizawa, *J. Cryst. Growth*, **208**, 416 (2000)
- [29] K. Tanaka, Y. Miyamoto, H. Uchiki, K. Nakazawa, and H. Araki, *Phys. Stat.Sol. (a)* **203**, 2891 (2006).